J. Membrane Biol. 89, 211–223 (1986)

The Journal of
Membrane Biology

Binding of Chloride and a Disulfonic Stilbene Transport Inhibitor to Red Cell Band 3

James A. Dix†, A.S. Verkman*, and A.K. Solomon

Biophysical Laboratory, Department of Physiology and Biophysics, Harvard Medical School, Boston, Massachusetts 02115 and
† Department of Chemistry, State University of New York, Binghamton, New York 13901

Summary. The effect of chloride on 4,4′-dibenzamido-2,2′-disulfonic stilbene (DBDS) binding to band 3 in unsealed red cell ghost membranes was studied in buffer [NaCl (0 to 500 mM) + Na citrate] at constant ionic strength (160 or 600 mM), pH 7.4, 25°C. In the presence of chloride, DBDS binds to a single class of sites on band 3. At 160 mM ionic strength, the dissociation constant of DBDS increases linearly with chloride concentration in the range [Cl] = 10 to 120 mM; at 600 mM ionic strength, the DBDS dissociation constant saturates hyperbolically with half-saturating [Cl] = 450 mM. The observed rate of DBDS binding to ghost membranes, as measured by fluorescence stopped-flow kinetic experiments, increases with chloride concentration at both 160 and 600 mM ionic strength. The equilibrium and kinetic results have been incorporated into the following model of the DBDS-band 3 interaction:

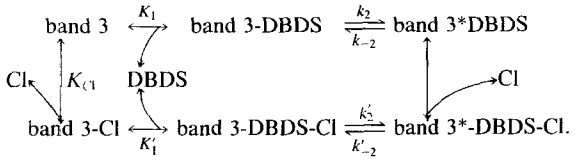

The equilibrium and rate constants of the model at 600 mM ionic strength are $K_1 = 0.67 \pm 0.16$ μM, $k_2 = 1.6 \pm 0.7$ sec^{-1}, $k_{-2} = 0.17 \pm 0.09$ sec^{-1}, $K_1' = 6.3 \pm 1.7$ μM, $k_2' = 9 \pm 4$ sec^{-1} and $k_{-2}' = 7 \pm 3$ sec^{-1}. The apparent dissociation constants of chloride from band 3, K_{Cl}, are 40 ± 4 mM (160 mM ionic strength) and 11 ± 3 mM (600 mM ionic strength). Our results indicate that chloride and DBDS have distinct, interacting binding sites on band 3.

Key Words red cell · anion transport · disulfonic stilbene · band 3

Introduction

Human red cell anion exchange is mediated by a 95,000 dalton glycoprotein, band 3, which is present as about 550,000 noncovalent dimers (Steck, 1978). A number of disulfonic stilbene compounds are potent, specific inhibitors of anion exchange and have been used to characterize the structure and function of band 3 (Cabantchik et al., 1978; Knauf, 1979). The stilbene inhibitor, DBDS (4,4′-dibenzamido-2,2′-disulfonic stilbene), undergoes a 100-fold fluorescence enhancement when bound to band 3 (Cabantchik & Rothstein, 1972; Rao et al., 1979). DBDS binds to approximately 1.1×10^6 sites on the red cell membrane; in the absence of chloride, binding occurs by a weak association of DBDS to one band 3 monomer (dissociation constant $K_1 = 3$ μM), followed by a conformational change (forward rate constant $k_2 = 4$ sec^{-1}, reverse rate constant $k_{-2} = 0.09$ sec^{-1}). A second DBDS molecule then binds to the second band 3 monomer ($K_3 = 0.85$ μM) in a sequential manner (Dix et al., 1979; Verkman et al., 1983), according to the following scheme:

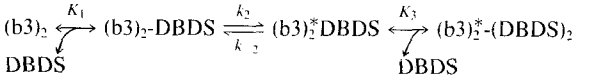

(1)

in which $(b3)_2$ represents a band 3 dimer and $(b3)_2^*$-DBDS represents the complex after the slow conformational change has taken place. Evidence has been presented indicating that the conformational change involves two band 3 monomers and modifies the characteristics of the second DBDS binding site.

In order to investigate the relationship between anion binding and stilbene inhibitor binding, we have studied the binding of DBDS to red cell ghost membranes in the presence of chloride. Chloride inhibits DBDS binding in equilibrium experiments and also increases the measured rate of DBDS binding in kinetic experiments in a concentration-dependent manner. A model for DBDS and chloride bind-

* *Present address:* Division of Nephrology, University of California, San Francisco, California 94143.

ing to separate, yet interacting sites on each band 3 monomer is presented.

Table of Symbols

Concentrations

$(b3)_2$	band 3 dimer
band 3, b3, $b3_o$	band 3 monomer with chloride or DBDS binding site facing the extracellular solution
$b3_i$	band 3 monomer with chloride or DBDS site facing the intracellular solution
$b3_oCl$	chloride bound to extracellular binding site on band 3
$b3_iCl$	chloride bound to intracellular binding site on band 3
DBDS, DB	DBDS
Cl, Cl_o	extracellular chloride concentration
Cl_i	intracellular chloride concentration
b3DB	DBDS bound to band 3 after bimolecular binding step
b3*DB	DBDS bound to band 3 after unimolecular step
b3DBCl	DBDS and chloride simultaneously bound to band 3, after bimolecular DBDS binding step
b3*DBCl	DBDS and chloride simultaneously bound to band 3, after unimolecular DBDS binding step

Equilibrium Constants

K_1	[b3][DB]/[b3DB]
K_2	[b3*DB]/[b3DB]
K_1'	[b3Cl][DB]/[b3DBCl]
K_2'	[b3*DBCl]/[b3DBCl]
K_{Cl_o}	$[b3_o][Cl_o]/[b3_oCl]$
K_{Cl_i}	$[b3_i][Cl_i]/[b3_iCl]$
K_{oi}	$[b3_oCl]/[b3_iCl]$
K_{eq}	[b3][DB]/([b3DB] + [b3*DB])
K_{eq}'	[b3Cl][DB]/([b3DBCl] + [b3*DBCl])
K_1^{app}	([b3] + [b3Cl])[DB]/([b3DB] + [b3DBCl])
K^{app}	([b3] + [b3Cl])[DB]/([b3DB] + [b3*DB] + [b3DBCl] + [b3*DBCl])
K_{Cl}^*	chloride concentration at which K^{app} half-saturates
$K_{(Cl_i=Cl_o)}$	-x intercept of Hunter-Downs plot when $[Cl_i] = [Cl_o]$
$K_{(Cl_i \gg Cl_o)}$	-x intercept of Hunter-Downs plot when $[Cl_i] \gg [Cl_o]$

Rate Constants

k_2	b3DB → b3*DB
k_{-2}	b3DB ← b3*DB
k_2'	b3DBCl → b3*DBCl
k_{-2}'	b3DBCl ← b3*DBCl
k_2^{app}	b3DB + b3DBCl → b3*DB + b3*DBCl
k_{-2}^{app}	b3DB + b3DBCl ← b3*DB + b3*DBCl
k_{Cl}^*	chloride concentration at which $(k_2^{app} + k_{-2}^{app})$ half-saturates

Materials and Methods

DBDS was synthesized by the method of Kotaki et al. (1971) and its purity was checked by thin-layer chromatography on Silica Gel G in pyridine/acetic acid/water (10:1:40). DBDS was stored as a 1-mM aqueous solution at 4°C in the dark. Previous studies have shown that DBDS does not undergo significant *cis-trans* isomerization during storage or under our experimental conditions (Verkman et al., 1983).

Hemoglobin-free unsealed red cell ghosts were prepared by a method similar to that of Dodge et al. (1963). Recently outdated blood was washed three times in 155 mM NaCl, hemolyzed in 5 mM Na phosphate at 0°C, pH 8.0, then washed four times in 5 mM Na phosphate buffer, and then washed twice in the buffer used for subsequent experiments. Ghosts were generally used within 24 hr of preparation, although longer storage up to 72 hr did not affect the results of kinetic experiments. Protein concentration was measured by the method of Lowry et al. (1951). The size distribution of washed ghosts was measured using a fluorescence-activated cell sorter (FACS II, Becton-Dickinson, Sunnyvale, Calif.). A single, Gaussian size distribution was found for washed ghosts in buffers containing Na citrate (28.5 mM) or NaCl (128 mM) + Na citrate (5 mM).

Buffers used for binding and kinetic experiments consisted of NaCl and Na citrate at pH 7.40. Buffer ionic strength was kept fixed at 160 mM (28.5 mM Na citrate) or 600 mM (108 mM Na citrate).

Equilibrium Binding Experiments

Equilibrium binding of DBDS to red cell ghost membranes was determined at 25°C by the fluorescence enhancement technique or the centrifugation technique described previously (Verkman et al., 1983). The fluorescence of a ghost solution (0.04 mg/ml total protein) was measured (excitation 350 nm, emission 427 nm) in a fluorescence spectrometer (MFP-2A, Perkin-Elmer, Norwalk, Conn.). Additions of DBDS to the ghost solution gave concentrations ranging from 0.02 to 5 μM. The measured fluorescence intensity was assumed to be proportional to the concentration of bound DBDS after corrections were made for inner filter effects, scattering and fluorescence of free DBDS, as described in the Appendix.

We have shown previously that DBDS binding to ghosts was completely abolished when ghost band 3 was labeled irreversibly with DIDS (4,4'-diisothiocyano-2,2'-disulfonic stilbene) in buffer consisting of 28.5 mM Na citrate (Verkman et al., 1983). A similar experiment was performed to determine whether there were any sites for DBDS binding to ghost band 3 at high chloride concentrations that could not be blocked by DIDS pretreatment. DBDS binding to ghosts was measured by the fluorescence enhancement technique using ghosts prepared from intact red cells covalently labeled with DIDS in buffer consisting of 28.5 mM Na citrate + 450 mM NaCl. At the highest DBDS concentration, 5 μM, DIDS treatment blocked more than 95% of DBDS binding to band 3, indicating that chloride does not make new DBDS sites available.

Kinetic Experiments

Stopped-flow experiments were performed by mixing 1.0 ml of a ghost solution (0.04 mg/ml total protein) with 1.0 ml of a solution

containing known DBDS concentrations; the binding time course was measured by fluorescence (excitation 350 nm, emission > 400 nm). Data were stored on a waveform recorder (model 805, Biomation, Cupertino, Calif.) and transferred to a PDP 11/34 computer (Digital Equipment, Maynard, Mass.) for storage and analysis.

Results

Equilibrium Binding

We have reported previously that DBDS binds to high (65 nM) and low (820 nM) affinity sites on band 3, in buffer consisting of 28.5 mM Na citrate, pH 7.4, 25°C (Verkman et al., 1983). Equilibrium binding and binding kinetics of DBDS to band 3 were characterized in the absence of transportable anions to serve as a benchmark against which effects of other inhibitors and buffers could be compared. The curve for [Cl] = 0 in the top portion of Fig. 1 displays the fitted binding curve for data obtained by centrifugation and reported previously using the sequential binding mechanism given in Eq. (1) and the binding affinities given above. The x intercept gives the total binding stoichiometry, 3.2 ± 0.3 nmol/mg ghost protein, which is equivalent to 1.0×10^6 sites per red cell membrane, assuming 5.1×10^{-10} mg protein/ghost cell (Lepke et al., 1976).

The data for [Cl] = 130 mM in the top portion of Fig. 1 were also obtained by the centrifugation method in which the concentration of bound DBDS is determined from the difference between total added DBDS and free DBDS measured in the supernatant after separation of ghosts by centrifugation. The decreased slope in the Scatchard plot indicates that chloride decreases the affinity of ghost band 3 for DBDS. The x intercept for the [Cl] = 130 mM curve is 3.3 ± 0.3 nmol/mg ghost protein, similar to that for the [Cl] = 0 curve, confirming that chloride does not affect the total number of DBDS binding sites on red cell band 3, as shown in Materials and Methods. As will be shown by the fluorescence enhancement binding method, more than one binding affinity cannot be resolved in the presence of chloride; when the [Cl] = 130 mM data is interpreted on the basis of a single site model, the fitted dissociation constant is 1.2 ± 0.2 μM.

The fluorescence enhancement titrations shown in the bottom portion of Fig. 1 give binding affinities but do not give values for site stoichiometry. The Scatchard representation of the fluorescence data was obtained by setting the stoichiometry at 3.2 nmol/mg ghost protein. The data are shown for [Cl] = 0 and 50 mM in buffer containing Na citrate at constant 600 mM ionic strength. Although the cur-

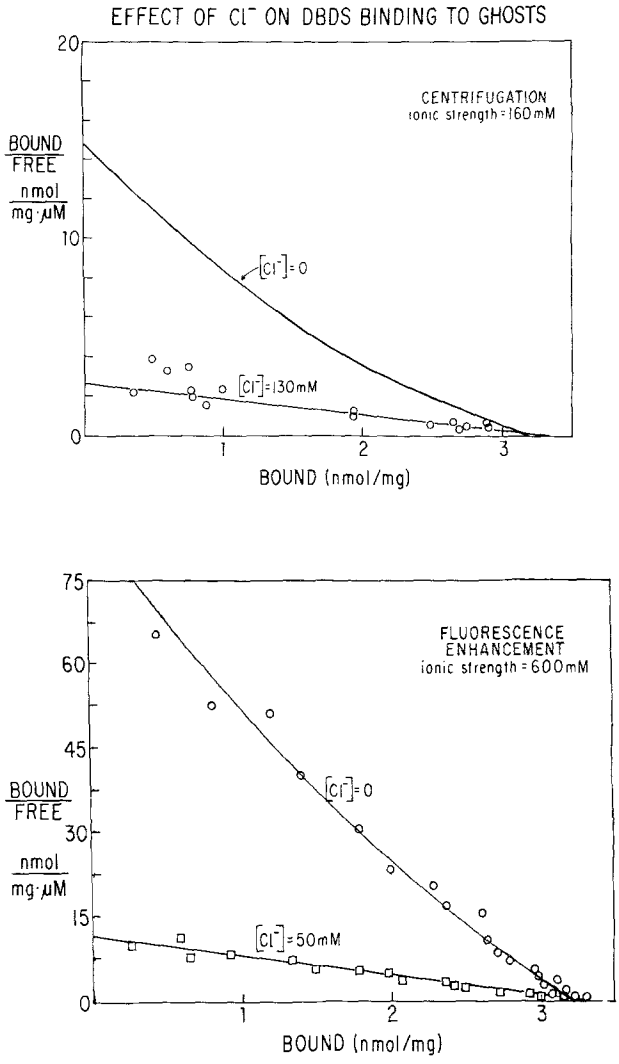

Fig. 1. Effect of chloride on DBDS binding to red cell ghost membranes. Top: Binding data using the centrifugation method. Known concentrations of ghosts and DBDS were incubated for 30 min at 25°C, pH 7.4, in buffer consisting of 0 or 130 mM NaCl and Na citrate at 160 mM constant ionic strength. The quantity of bound DBDS was determined from the difference between total DBDS and unbound supernatant DBDS measured by absorbance (molar absorptivity = 50,000 M^{-1} cm^{-1} at 336 nm) or by fluorescence upon addition of ghosts (excitation = 350 nm; emission = 420 nm) after centrifugation at 40,000 × g for 30 min. Results are shown in the form of a Scatchard plot. The curve for [Cl] = 0 is that given previously (Verkman et al., 1983) to the two-site sequential binding mechanism which characterizes DBDS binding in the absence of chloride (stoichiometry = 3.2 ± 0.3 nmol/mg ghost protein). The [Cl] = 130 mM curve is a nonlinear least-squares fit to a single-site model with K_{eq} = 1.2 ± 0.2 μM and stoichiometry = 3.3 ± 0.3 nmol/mg ghost protein (r = 0.97). Bottom: Binding data obtained using the fluorescence enhancement technique for 0 and 50 mM chloride at a constant 600 mM ionic strength are displayed in the form of a Scatchard plot. The fitted curve for [Cl] = 0 is a fit to the two-site sequential binding mechanism and the curve for [Cl] = 50 mM is a single-site fit

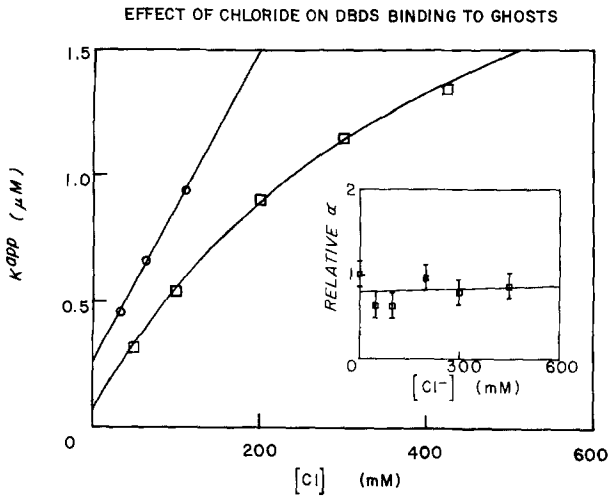

Fig. 2. Effect of [Cl] on equilibrium DBDS binding to ghosts. The fitted equilibrium dissociation constants, K^{app}, obtained by the fluorescence enhancement technique, are plotted as a function of [Cl] for 160 mM (○) and 600 (□) mM ionic strength. The 160 mM ionic strength data were fit to a straight line with slope = 0.0062 ± 0.0002 μM/mM and y intercept 0.25 ± 0.02 μM. The 600 mM ionic strength data were fit by nonlinear least-squares to a single, saturable site model, $K^{app} = A[Cl]/(K^*_{Cl} + [Cl]) + B$ (*see text*), with $A = 2.7 \pm 0.7$ μM, $B = 0.067 \pm 0.008$ μM, and $K^*_{Cl} = 450 \pm 50$ mM. The $-x$ intercept for the 160 mM ionic strength data is 40 ± 4 mM; the $-x$ intercept for the 600 mM ionic strength data is 11 ± 3 mM. Insert: The relative quantum yield of bound DBDS (α; *see* Verkman et al., 1983) is plotted as a function of [Cl]. The fitted line was obtained by weighted least-squares and has a slope of $(1.4 \pm 4.7) \times 10^{-4}$ mM^{-1}, not significantly different from zero

vature in the [Cl] = 0 data allows resolution of two distinct binding affinities, data for [Cl] = 50 mM, as well as for other nonzero chloride concentrations tested (30 to 450 mM), fall systematically along a single straight line (r = 0.97 to 0.99). An attempted fit of the [Cl] = 50 mM data to a two-site sequential binding model using the nonlinear Newton's method did not converge, supporting the inability to resolve more than one binding site in the presence of chloride.

In the presence of chloride, therefore, a single class of sites can be resolved with total stoichiometry equal to that for the [Cl] = 0 case, in which two sites are resolvable. There are several possible explanations for this finding. One explanation could be that chloride competes with only the high-affinity DBDS binding site. As the chloride concentration increases, the dissociation constant of the high-affinity site would approach the dissociation constant of the low-affinity site, and two sites would not be resolved in the Scatchard plot. However, as the chloride concentration increases still further, the binding mechanism would change from a negative cooperative mechanism to a positive cooperative mechanism, corresponding to Scatchard plots concave downward. Linear Scatchard plots were observed for all chloride concentrations (30 to 450 mM), so that chloride-DBDS competition at only the high-affinity site is unlikely.

A second explanation for the finding of a single class of DBDS binding sites in the presence of chloride could be that chloride competes with DBDS at only the low-affinity site. The low-affinity site would be shifted to such low affinity that it would not be probed with the DBDS concentrations employed. This explanation is unlikely, since the remaining site would be the high-affinity site with dissociation constant 65 nM, and would remain unaffected by chloride, contrary to what is observed (Fig. 1). Furthermore, the total site stoichiometry in the presence of chloride would be less than the stoichiometry in the absence of chloride, again contrary to what is observed (Fig. 1).

The transition from an interacting site model to a noninteracting site model can be explained by assuming that dimers of band 3, in the absence of chloride, are in a state different from dimers in the presence of chloride. In the absence of chloride, the two DBDS binding sites, one on each band 3 monomer, can interact; addition of chloride would change the band 3 dimer conformation so that interaction between DBDS binding sites is no longer possible. This model is discussed further in the Model section of this paper. While more complicated models could be devised to explain the results of our equilibrium binding experiments, the model presented in this paper provides a self-consistent explanation not only for the results of equilibrium experiments, but also for the results of our kinetic experiments.

Figure 2 shows the apparent DBDS dissociation constant, K^{app}, as a function of [Cl] using the fluorescence enhancement titration technique.[1] For 600 mM ionic strength, there is approximate linearity between the apparent DBDS dissociation constant and chloride concentration for [Cl] < 200 mM, but

[1] The formally correct plot for Fig. 2 would be K_{app} versus chloride activity rather than chloride concentration. We have measured the mean sodium chloride activity coefficient in the chloride/citrate buffer used in our experiments; the activity was estimated with a silver/silver chloride electrode (Brown, 1934) referenced to reported values of mean sodium chloride activity coefficients of sodium chloride solutions (Robinson & Stokes, 1959). Surprisingly, the mean activity coefficient of the sodium chloride/sodium citrate buffer was identical to that of a sodium chloride solution over the range [Cl] = 50 to 600 mM. If the chloride activity coefficient is taken as the mean activity coefficient, then a plot of K_{app} versus chloride activity is still hyperbolic, as in Fig. 2, with half-saturation at [Cl] = 340 mM.

at higher chloride concentrations the data deviate from linearity. A rectangular hyperbola of the form

$$K^{app} = A[Cl]/(K^*_{Cl} + [Cl]) + B \quad (2)$$

can be fitted to the 600 mM ionic strength data in which $A = 2.7 \pm 0.7$ μM, $B = 0.067 \pm 0.008$ μM and $K^*_{Cl} = 450 \pm 50$ mM. The parameter K^*_{Cl} is the chloride concentration at which the effect of chloride on the apparent equilibrium dissociation constant of DBDS half-saturates. The nonlinear dependence of K^{app} on chloride concentration demonstrates that simple competition between chloride and DBDS cannot provide a full description for the effects of chloride on DBDS binding to ghosts. Equation (2) is derived from a saturable binding model, in which DBDS and chloride possess separate, interacting sites, and both sites can be occupied simultaneously.

For 160 mM ionic strength, the data appear to fall along a straight line, consistent with DBDS and chloride competition for a single class of binding sites on band 3. The apparent inhibition constant for chloride, determined as the $-x$ intercept of a linear fit through the data in Fig. 2, is 41 ± 3 mM. The extrapolated dissociation constant for DBDS at [Cl] = 130 mM is 1.1 μM, similar to the 1.2 μM dissociation constant determined by the centrifugation method (Fig. 1, top).

The insert to Fig. 2 shows the calculated values of α, the relative quantum yield of bound DBDS, as determined by the fluorescence binding method described in the appendix to Verkman et al. (1983). The slope of the α *vs.* [Cl] plot does not differ significantly from zero, suggesting that the maximum amount of DBDS bound to ghosts is not a function of [Cl]. This is consistent with the similar total site stoichiometry for [Cl] = 0 (3.2 nmol/mg ghost protein) and [Cl] = 130 mM (3.3 nmol/mg ghost protein) in the centrifugation binding data shown in the top of Fig. 1.

Binding Kinetics

When DBDS is mixed with red cell ghost membranes in a stopped-flow experiment, the fluorescence increases with time as shown in Fig. 3, corresponding to the time course of DBDS binding to ghosts (Verkman et al., 1983). In the presence of chloride, the exponential time constant for the binding process decreases; as shown in Fig. 3, 90 mM NaCl increased the observed binding rate by a factor of three.

A useful way to display kinetic data for the DBDS-band 3 interaction is to plot τ *vs.* $[DBDS]^{-1}$ as in Fig. 4, in which τ is the exponential time constant for the reaction time course. A bimolecular step followed by a rate-limiting conformational change, using the notation in Eq. (1), can be written as

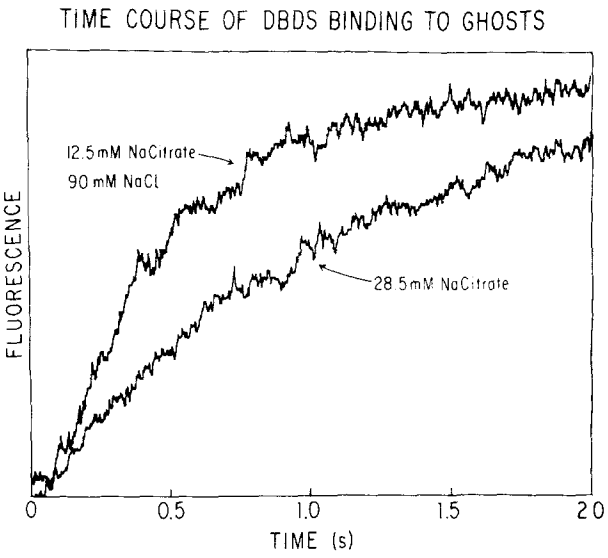

Fig. 3. Time course of DBDS binding to ghosts. 1.0 ml of 1 μM DBDS was mixed with 1.0 ml of a 0.04 mg/ml ghost solution in a stopped-flow experiment in buffer consisting of 28.5 mM Na citrate or 12.5 mM citrate + 90 mM NaCl, pH 7.4, 23°C. The time course of DBDS binding to ghost band 3 was followed by measuring fluorescence (excitation = 350 nm; emission > 400 nm). The fluorescence scale is in arbitrary units; the two time courses are scaled so that the total amplitudes are equal. Fitted time constants for a single exponential fit to the time course are 1.2 ± 0.2 sec (28.5 mM citrate) and 0.42 ± 0.07 sec (90 mM NaCl)

$$\text{band 3} \overset{K_1}{\rightleftharpoons} \text{band 3-DBDS} \underset{k_{-2}}{\overset{k_2}{\rightleftharpoons}} \text{band 3*-DBDS}. \quad (3)$$
$$\text{DBDS}$$

The predicted relationship between τ and [DBDS] for Eq. (3) is (Eigen & DeMayer, 1974)

$$\tau = (k_{-2} + k_2[DBDS]/(K_1 + [DBDS]))^{-1}. \quad (4)$$

Equation (4) predicts that the value of the stopped-flow time constant, extrapolated to infinite [DBDS], is equal to the reciprocal of the sum of the forward and reverse rate constants of the conformational change, $(k_2 + k_{-2})^{-1}$. The value of τ corresponding to infinite [DBDS] can be obtained as the y intercept of a plot of τ *vs.* 1/[DBDS], as in Fig. 4.

If it is assumed that the mechanism in Eq. (3) applies when chloride is present, provided that K_1, k_2 and k_{-2} are functions of chloride (K_1^{app}, k_2^{app} and

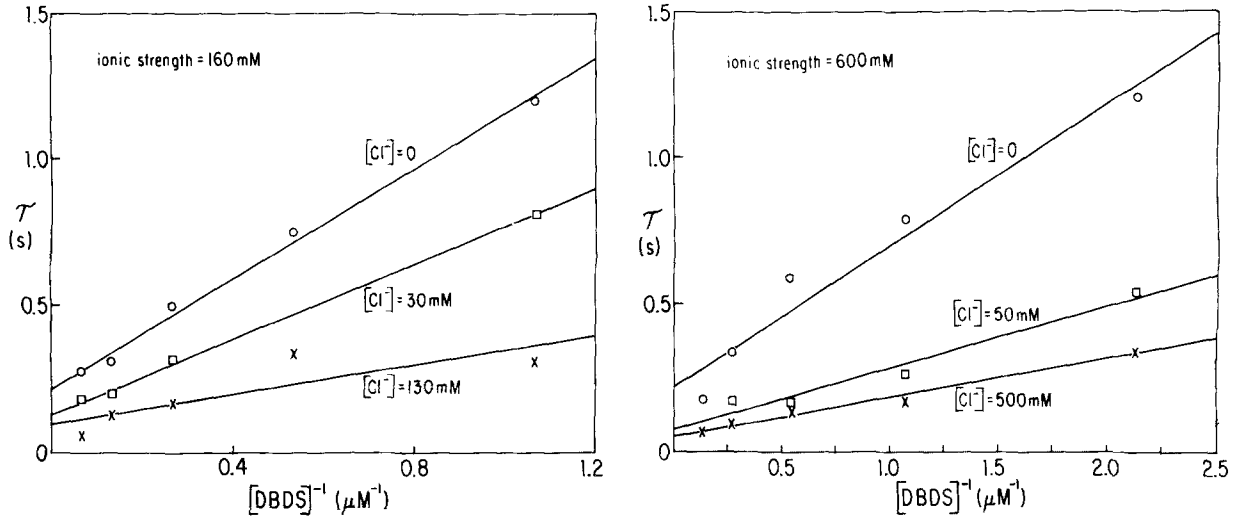

Fig. 4. Effect of Cl on band 3-DBDS binding kinetics. Concentration dependence of stopped-flow time constants for DBDS binding to ghost membranes. The abscissa values represent reciprocal total DBDS concentrations. The ordinate is the fitted single exponential time constant obtained from the measured time course of DBDS binding to ghosts. Each point is an average of experiments performed in quadruplicate; errors (*not shown*) were in the range of 10 to 20%. The fitted reciprocal intercepts ($k_2^{app} + k_{-2}^{app}$) obtained from weighted least-squares fits to the data are shown in Fig. 5. Left: Data is shown for 0, 30 and 130 mM [Cl] at 160 mM ionic strength. Right: Data is shown for 0, 50 and 500 mM [Cl] at 600 mM ionic strength

k_{-2}^{app}), then an equation analogous to Eq. (4) can be written

$$\tau = (k_{-2}^{app} + k_2^{app}[DBDS]/(K_1^{app} + [DBDS]))^{-1}. \quad (5)$$

Values of τ, obtained in the presence of chloride and extrapolated to infinite [DBDS], are approximately equal to $(k_2^{app} + k_{-2}^{app})^{-1}$. Although $(k_2^{app} + k_{-2}^{app})$ is relatively well determined by plots as in Fig. 4, K_1^{app} is not well determined because it depends upon the detailed dependence of τ *vs.* 1/[DBDS].

Figure 5 shows the dependence of $(k_2^{app} + k_{-2}^{app})$ on chloride concentration. The values of $(k_2^{app} + k_{-2}^{app})$ were obtained as the reciprocal τ values extrapolated to infinite [DBDS] as described above. As shown in Fig. 5, $(k_2^{app} + k_{-2}^{app})$ increases from 1.7 sec^{-1} to 16 sec^{-1} with half-point of [Cl] = 40 ± 12 mM. Data for low ionic strength (*not shown*) generally fall within 2 SD of the fitted line in Fig. 5. The chloride concentration at which the half-maximal change in $(k_2^{app} + k_{-2}^{app})$ occurs, 40 mM, is very different from the half-concentration, 450 mM, for the chloride effect on equilibrium DBDS binding to ghosts.

Since the values of $(k_2^{app} + k_{-2}^{app})$ in Fig. 5 increase with increasing [Cl], chloride accelerates the apparent rate constants, $(k_2^{app} + k_{-2}^{app})$, for the band 3-DBDS conformational change. If chloride and DBDS were to compete simply for a single binding site, each line in Fig. 4 should have the same intercept on the *y* axis. Furthermore, at any DBDS concentration, τ should increase with increasing [Cl], rather than decrease, if there were simple competition, as observed for simple competition between the inhibitor phloretin and DBDS on band 3 (Forman et al., 1982).

Model

In this section, a model is presented which incorporates the quantitative observations given in the Results section. As already pointed out, the saturating behavior of K^{app} and $(k_2^{app} + k_{-2}^{app})$, and the increase in $(k_2^{app} + k_{-2}^{app})$ with chloride (Figs. 2, 4 and 5) indicate that simple competition between chloride and DBDS for a single binding site cannot account for the data. A mechanism in which chloride and DBDS possess distinct binding sites has been incorporated into the following model:

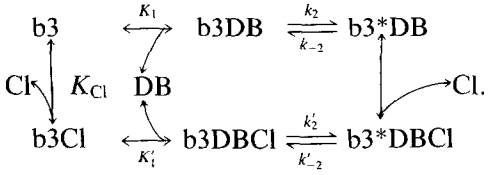

(6)

The equilibrium constants of the model are defined as follows:

$$K_1 = [b3][DB]/[b3DB] \quad K'_1 = [b3Cl][DB]/[b3DBCl]$$
$$K_2 = k_2/k_{-2} = [b3^*DB]/[b3DB]$$
$$K'_2 = k'_2/k'_{-2} = [b3^*DBCl]/[b3DBCl]$$
$$K_{Cl} = [b3][Cl]/[b3Cl]$$
$$K_{eq} = K_1/(1 + K_2) = [b3][DB]/([b3^*DB] + [b3DB])$$
$$K'_{eq} = K'_1/(1 + K'_2) = [b3Cl][DB]/([b3DBCl] + [b3^*DBCl])$$
$$K^{app} = ([b3] + [b3Cl])[DB]/([b3DB] + [b3DBCl] + [b3^*DB] + [b3^*DBCl]). \quad (7)$$

The equilibrium constant for the bimolecular chloride binding step at the right in Eq. (6) need not be defined independently since its value is determined from the remaining parameters in the cyclic reaction scheme. The equilibrium and rate constants that are not primed represent DBDS binding parameters in the absence of chloride, while those that are primed represent binding parameters in the presence of chloride.

The model presented in Eq. (6) incorporates the results presented in the previous section. In the absence of chloride, DBDS can bind to band 3 by the upper pathway as shown previously (Verkman et al., 1983). As chloride is added, DBDS can also bind by the bottom pathway. The rate of DBDS binding in the bottom pathway is faster than the binding rate in the top pathway; therefore chloride increases the rate of DBDS binding. The saturating behavior of equilibrium and rate constants is expected from the model, since at infinite chloride, DBDS can bind only by the bottom pathway. Finally, the increase in the dissociation constant for DBDS, K^{app}, seen with chloride (Fig. 2) is predicted if $K'_{eq} > K_{eq}$, as will be shown below.

The mechanism in Eq. (6) incorporates a single class of binding sites for DBDS, in contrast to two classes of binding sites measured by Verkman et al. (1983) for DBDS binding in the absence of chloride. We propose that in the absence of chloride, two monomers of a band 3 dimer can interact, but that in the presence of chloride, the monomers act independently with respect to DBDS binding. The transition from interacting to noninteracting monomers could be incorporated formally in the model of Eq. (6) by including a second, high-affinity chloride binding site. At the lowest chloride concentration used in this study (10 mM), this second binding site would be completely saturated, converting all of the band 3 dimers from interacting to noninteracting monomers. Although other explanations are possible to describe the transition from a two-site binding mechanism in the absence of chloride to a one-site binding mechanism in the presence of chloride, our explanation provides a useful conceptual framework in which to discuss the results of our equilibrium and kinetic data.

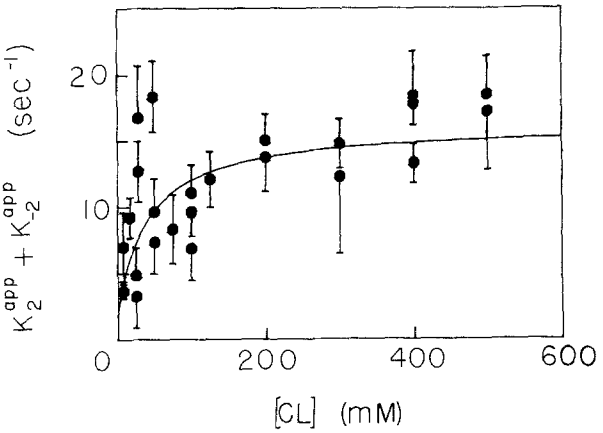

Fig. 5. Effect of chloride on $k_2^{app} + k_{-2}^{app}$). The $(k_2^{app} + k^{app}{}_2)$ values, obtained from the reciprocal y intercept from kinetic plots as shown in Fig. 4 for 600 mM ionic strength, are shown as a function of [Cl]. Error bars represent one SD. The fitted curve is obtained from the nonlinear least-squares fit to a single, saturable site model, $(k_2^{app} + k_{-2}^{app}) = A[Cl]/(k_{Cl}^* + [Cl]) + B$, with $A = 14 \pm 1$ sec^{-1}, $B = 1.7 \pm 0.5$ sec^{-1} and $k_{Cl}^* = 40 \pm 12$ mM. At [Cl] = 0, $(k_2^{app} + k_{-2}^{app}) = k_2 + k_{-2} = B$; at [Cl] = ∞, $(k_2^{app} + k_{-2}^{app}) = k'_2 + k'_{-2} = A + B$

There are seven independent parameters which characterize the mechanism given in Eq. (6). K_1, k_2 and k_{-2} apply in the absence of chloride, K'_1, k'_2 and k'_{-2} apply in the presence of chloride, and K_{Cl} is the chloride binding constant which "proportions" DBDS binding between the upper and lower pathways in the mechanism. The strategy which will be used to evaluate the seven independent parameters is as follows.

Equilibrium binding constants (Fig. 2) extrapolated to [Cl] = 0 give a value for K^{app} in the absence of chloride; in this limit, K^{app} gives the combination of parameters

$$K_{eq} = K_1/(1 + k_2/k_{-2}) \quad (8)$$

as given in Eq. (6).

The limiting value of K^{app} as chloride goes to infinity gives the combination of parameters

$$K'_{eq} = K'_1/(1 + k'_2/k'_{-2}). \quad (9)$$

Table. Rate and equilibrium constants for DBDS binding to band 3

Extrapolated to [Cl] = 0, 600 mM ionic strength		
K_1	0.67 ± 0.16	μM
k_2	1.6 ± 0.7	sec^{-1}
k_{-2}	0.17 ± 0.09	sec^{-1}
K_{eq}	0.067 ± 0.008	μM
Extrapolated to [Cl] = ∞, 600 mM ionic strength		
K_1'	6.3 ± 1.7	μM
k_2'	9.0 ± 3.5	sec^{-1}
k_{-2}'	7.0 ± 2.8	sec^{-1}
K_{eq}'	2.8 ± 0.7	μM
Chloride dissociation constants		
K_{Cl}	11 ± 3	mM (600 mM ionic strength)
	40 ± 4	mM (160 mM ionic strength)

K_{Cl} is determined in Fig. 2 from the value of [Cl], K_{Cl}^*, at which K^{app} half-saturates:

$$K_{Cl}^* = K_{Cl}K_{eq}'/K_{eq}. \tag{10}$$

Equation (10) is derived as described in the Appendix. The limiting value of $(k_2^{app} + k_{-2}^{app})$ in Fig. 5, as chloride goes to infinity, gives the value of $k_2' + k_{-2}'$; the extrapolated value of $(k_2^{app} + k_{-2}^{app})$ at zero chloride gives the value of $k_2 + k_{-2}$.

The two remaining independent parameters, K_1 and K_1', are determined from a fit of τ as a function of DBDS and chloride concentration. The fitting function, as derived in the Appendix, is

$$\tau = \frac{\left[\frac{K_2}{K_1} + \frac{K_2'[Cl]}{K_1'K_{Cl}}\right]\left[1 + [DBDS]\frac{1}{K_1} + \frac{[Cl]}{K_1'K_{Cl}} + \frac{[Cl]}{K_{Cl}}\right]}{\left[\frac{k_2}{K_1} + \frac{k_2'[Cl]}{K_1'K_{Cl}}\right]\left[1 + [DBDS]\frac{1}{K_{eq}} + \frac{[Cl]}{K_{eq}'K_{Cl}} + \frac{[Cl]}{K_{Cl}}\right]}. \tag{11}$$

Equation (11) was fit by the iterative, nonlinear least-squares method to eighty values of τ at DBDS concentrations between 0.5 and 8 μM and Cl concentrations between 10 and 500 mM at constant ionic strength of 600 mM. For the fit, $(k_2 + k_{-2})$, $(k_2' + k_{-2}')$, K_{eq}, K_{eq}' and K_{Cl} were held fixed at values determined as described above, and K_1 and K_1' were allowed to vary. Once the best-fit values of K_1 and K_1' were determined, values for k_{-2} and k_{-2}' were calculated from Eqs. (7) and (8). A summary of the rate and equilibrium constants describing the mechanism in Eq. (6) is given in the Table.

In the analysis of the stopped-flow time constants, we have assumed that the bimolecular step in DBDS binding in the presence of chloride is much more rapid than the unimolecular step (as is the case in the absence of chloride), so that this step can be described by an equilibrium constant rather than two rate constants. This assumption is justified based on unpublished work of Smith and Dix, who found that, in the presence of chloride, the stopped-flow time constants for the bimolecular step are appreciably faster than those for the unimolecular step.

Discussion

Fröhlich (1982) has studied the effects of chloride on the binding of DNDS (4,4′-dinitro-2,2′-disulfonic stilbene) to intact red cells at varying ionic strength. In the presence of 20 to 100 mM chloride, equal on both sides of the membrane, a single DNDS binding site was observed, in agreement with our results for DBDS binding with 30 to 450 mM chloride in unsealed ghosts. Fröhlich determined K_{Cl} = 39 ± 4 mM from a plot of the apparent DNDS binding constant *vs.* chloride, identical to Fig. 2 in the present paper; this value is in excellent agreement with our value of K_{Cl} = 40 ± 4 mM.

Shami et al. (1978) and Knauf (1979) have concluded, on the basis of the linearity of the Hunter-Downs plot of inhibition of chloride self-exchange by stilbene inhibitors, that stilbenes compete with anions at a single binding site on band 3. Anion transport inhibition results from displacement of chloride from its transport binding site. If the anion site probed by our experiments with DBDS is indeed the transport site, and if chloride and DBDS were to displace each other from that site, then chloride should have decreased the observed rate of DBDS binding. Furthermore, the downward concavity of K^{app} in Fig. 2 implies that as [Cl] $\rightarrow \infty$, DBDS binding is still possible. This behavior is not consistent with simple competitive inhibition.

The model incorporates both a chloride binding site and a DBDS binding site but makes no provision for a modifier site. The modifier site has been proposed by Dalmark (1976) to account for the self-inhibition of chloride exchange at high chloride concentrations and would thus be an alternative explanation for the saturation in Fig. 2. The modifier site is thought to be a low-affinity binding site for anions (300 mM for Cl) located on the intracellular surface (Knauf & Mann, 1984*a*), distinct from the anion binding site involved in anion transport, which has a higher affinity (4 to 60 mM for chloride).

The curved plot of K^{app} *vs.* chloride in Fig. 2 has a half-point of 450 mM, similar to the 300 mM half-point for the proposed binding of chloride to the band 3 modifier site, so that in this respect, a chloride modifier site, rather than the chloride transport

site, could be responsible for the curvature in Fig. 2. Although it is possible to imagine that chloride bound to the modifier site can both accelerate the rate of the band 3-DBDS conformational change in the manner shown in Fig. 5 and decrease the DBDS binding affinity to band 3 as shown in Fig. 2, a quantitative examination of the kinetic data in Fig. 5 rules this out.

Two cases need to be considered. In the first case, binding of chloride to the modifier site would be unaffected by the presence of DBDS on the DBDS binding site. This condition would be necessary since the 450 mM half-point in Fig. 2 would, in this case, be a measure of the modifier site affinity for chloride which has a 300-mM affinity. All effects of chloride bound at the modifier site on DBDS equilibrium binding and binding kinetics should therefore have half-saturating values of 300 to 450 mM. However, the half-saturating value for the chloride effect on DBDS binding kinetics is 40 mM as given in Fig. 5, which is inconsistent with chloride action at the modifier site, when chloride binding is unaffected by DBDS.

A second possibility is that the chloride binding site for the DBDS interaction is the modifier site. In this case, the observed effects of chloride on DBDS binding to band 3 would probe the modifier site rather than the chloride transport site. However, as the Table shows, the K_{Cl} value of 11 mM is not consistent with the modifier site affinity of 300 mM. These arguments demonstrate that DBDS and chloride interactions with a modifier site cannot account for the experimental observations. The data do not in any way support or refute the existence of a modifier site; a modifier site may well explain the self-inhibition of chloride self-exchange at high chloride, and have no effect on band 3-inhibitor interactions.

The conclusion that distinct binding sites for DBDS and chloride exist on band 3 does not specify the location of the chloride binding site. Nonetheless, several models can be excluded based on the data presented in the Results section of this paper. It may be possible, for example, that chloride present on one monomer of band 3 affects binding of DBDS to the transport site on the other monomer. In this manner, chloride could interact with DBDS in a general noncompetitive manner, with only a single transport site on each band 3 monomer. Such a scheme seems plausible on the basis of the interacting dimer mechanisms proposed by Macara and Cantley (1981), Salhany et al. (1981) and Verkman et al. (1983). The evidence against such an interaction of chloride on one monomer with DBDS bound to the transport site on the other monomer is the finding that K^{app} saturates to a finite value at high chloride concentration. If the chloride concentration is very large, no DBDS could remain bound to a transport site since chloride would compete with DBDS directly on the same monomer. Therefore, although an interaction between chloride on the transport site on one monomer and DBDS bound to its site on the other monomer cannot be ruled out, such an interaction cannot account for the data which show distinct, interacting chloride and DBDS sites.

Another plausible type of model is that DBDS binds to band 3 by a bipolar, two-site attachment. For example, one sulfonate of DBDS could bind to the DBDS binding site, which would then induce a conformational change corresponding to binding of the other sulfonate to the chloride binding site. This model would explain inhibition of DBDS binding with increasing chloride concentration and the saturable binding in Fig. 2. This bipolar model, however, is inconsistent with the observation that chloride increases the rate of DBDS binding. If chloride is present on the transport site, the conformational change would be effectively blocked, and the binding rate must decrease.

Relationship to Anion Exchange Data

Shami et al. (1978) studied the kinetics of inhibition of anion exchange by the dihydro analog of DIDS, H_2DIDS, and found that their data could be described by a linear Hunter-Downs plot over the concentration range [Cl] = 0 to 600 mM. Largely on this basis, they concluded that H_2DIDS inhibition occurs by a specific competitive interaction between the stilbene inhibitor and chloride at a single transport site. Our studies have been concerned with the binding of another stilbene inhibitor, DBDS, but not with the effect of DBDS on chloride exchange. In order to compare our results with the observations of Shami et al. (1978), we have assumed that the chloride site probed by DBDS is the transport site, and have added transport steps to the DBDS reaction mechanism as shown in Fig. 6, corresponding to the currently accepted "ping-pong" mechanism of anion transport (Gunn & Fröhlich, 1979). All of the chloride reaction steps are assumed to be fast so that any observed DBDS reaction time course is not rate-limited by chloride binding. The mechanism in Fig. 6 is a mixed-type inhibition mechanism (Segel, 1975). All of the DBDS reactions in the mechanism in Fig. 6 take place on the extracellular (outer) side of the membrane. In order to retain compatible notation, we will use the subscript i to denote the cytoplasmic (inner) side of the membrane and the subscript o to denote the outer side.

In studies of enzyme kinetics, the Hunter-

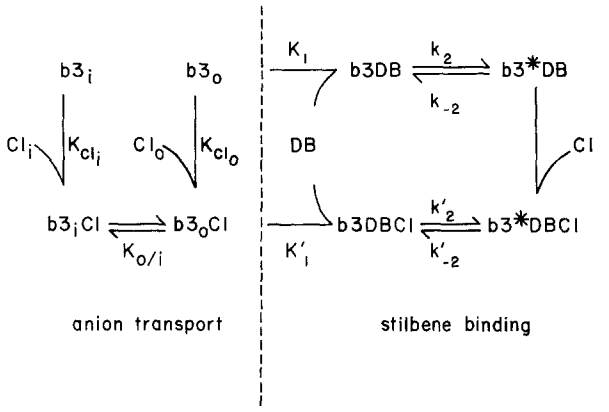

Fig. 6. Relation between DBDS binding and anion transport. Mechanism of inhibition of anion transport by DBDS. The reaction steps to the right of the dashed vertical line represent the interaction of chloride and DBDS on the extracellular surface of the membrane, as given in Eq. (6) of the text. The reaction steps to the left of the vertical line represent the "ping-pong" mechanism of anion transport

Downs plot shows the relation between $[I](1 - i)/i$ (where $[I]$ is inhibitor concentration and i is the fractional inhibition of transport) and substrate concentration. One feature of this method of presenting inhibition data is that the $-x$ intercept of the plotted function provides a measurement of the dissociation constant of the substrate. Shami et al. (1978) have studied an anion exchange system with several reaction steps and plotted their results according to the Hunter-Downs method.

The mechanism of their anion exchange system is given by the reaction steps on the left of the vertical dotted line in Fig. 6. Under these conditions, the $-x$ intercept gives an effective dissociation constant for chloride binding which contains contributions from K_{Cl_i}, K_{Cl_o} and K_{oi}. The complete expression for the Hunter-Downs plot has been derived in the Appendix both for the reaction mechanism of Fig. 6 and for the simpler mechanism in which inhibition is competitive as observed by Shami et al. (1978). In both cases, the expressions are complex, but they may be simplified at two experimental limits. When $[Cl]_i \gg [Cl]_o$, the $-x$ intercept of the Hunter-Downs plot is

$$K_{(Cl_i \gg Cl_o)} = K_{oi}K_{Cl_o}/(1 + K_{oi}). \quad (12)$$

when $[Cl]_i = [Cl]_o$ the equation for the $-x$ intercept is

$$K_{(Cl_i = Cl_o)} = (K_{oi}K_{Cl_o} + K_{Cl_i})/(1 + K_{oi}). \quad (13)$$

Both Eqs. (12) and (13) do not depend on whether the inhibition is competitive or mixed as shown in the Appendix. The reason is that the $-x$ intercept depends only upon equations to the left of the vertical dotted line in Fig. 6. By the same argument, the $-x$ intercept is independent of the nature of the inhibitor.

Although the $-x$ intercept of the Hunter-Downs plot is independent of the nature of the inhibitor and of the inhibition mechanism, the other characteristics of the Hunter-Downs plot depend upon both of these factors. As mentioned in the Appendix, since the y-axis in a Hunter-Downs plot is a measure of the apparent binding constant of the inhibitor, the predicted Hunter-Downs plot for the mechanism in Fig. 6 would be identical with the plot of equilibrium binding data presented in Fig. 2. However, the interpretation of the parameters of the fitted curve in Fig. 2 is now more complex by the inclusion of the reaction steps to the left of the vertical dotted line in Fig. 6. The $-x$ intercept is given by Eq. (13); the y intercept is equal to $K_{eq}(1 + K_{Cl_i}/K_{oi}K_{Cl_o})$, the chloride concentration at which K^{app} (or $[I](1 - i)/i$) half-saturates is equal to $K'_{eq}K_{Cl_o}/K_{eq}$, and K^{app} at infinite chloride is equal to $K'_{eq}(1 + 1/K_{oi})$.

As pointed out by Fröhlich (1982), binding or transport inhibition data taken when $[Cl_i] = [Cl_o]$ cannot be used to determine the parameters $K_{oi}K_{Cl_o}/K_{Cl_i}$ [the asymmetry factor, A, in the notation of Knauf et al. (1984)]. Reported values of A include 0.2 [obtained from the data of Barzilay et al. (1979) and Fröhlich (1982), as described by Knauf et al. (1984)] and a value of 0.067 [obtained from the data of Gunn and Fröhlich (1979)]. Based on studies with the noncompetitive transport inhibitor, niflumic acid, Knauf and Mann (1984*b*) have concluded that $K_{Cl_i} = K_{Cl_o}$ and $K_{oi} = 0.067$. If the asymmetry in the transport system does indeed arise solely from K_{oi}, then the value of K_{Cl} obtained from the $-x$ intercept of Fig. 2 represents the true dissociation constant of chloride from either side of the membrane; however, the DBDS dissociation constants in the absence and presence of chloride (K_{eq} and K'_{eq}) would be a factor of 16 lower than those reported in the Table.

The major difference between our predicted Hunter-Downs plots and the Hunter-Downs plot obtained by Shami et al. (1978) is that our plot would saturate at high chloride concentrations (with half-saturating chloride concentration given by $K_{Cl_o}K'_{eq}/K_{eq} = 450$ mM as in Fig. 2) while the plot obtained by Shami et al. was linear with chloride concentration and did not saturate. Although one may expect the rather bulky DBDS molecule to have an inhibition mechanism different from the smaller H_2DIDS molecule, several differences in experimental protocol preclude a detailed compari-

son of our predicted plots with those obtained by Shami et al. Our data were obtained at 25°C, at constant ionic strength, and using ghost membranes; Shami et al. obtained their data at 0°C, at varying ionic strength, and using intact red cells. Verkman et al. (1983) have found that increasing ionic strength increases the affinity of DBDS for binding to ghost membranes. If this were also true for H_2DIDS binding to intact cells, then the apparent inhibition constants of Shami et al., when corrected for ionic strength, would be lowered at low chloride concentrations, leading to a curvature in the Hunter-Downs plot and a lower value for the $-x$ intercept.

In the preceding discussion, we have assumed that the chloride site probed by DBDS is the transport site; although chloride and DBDS have separate sites, chloride can be transported only if DBDS is not bound to its site. There are other more complicated interactions between DBDS and chloride that would be consistent with our data. For example, chloride could interact competitively with DBDS at the transport site; the increase in binding rate (Fig. 4) and part of the decrease in binding affinity (Fig. 2) of DBDS to band 3 would then be explained by a second chloride site that could be bound simultaneously with DBDS. If the affinity of the second chloride site were less than the affinity of the first chloride site, then at low chloride concentrations, the inhibition of chloride transport by DBDS would be linear, as would inhibition at high chloride concentrations; the inhibition constants, however, would differ. The transition between the two regimes of inhibition would be moderated by chloride binding to the second site, giving apparent curvature to plots such as in Fig. 2 and in Hunter-Downs plots. A final explanation of the relation between DBDS inhibition and inhibition by other stilbenes will not be possible until the anion exchange kinetics have been characterized.

The data presented in this paper serve as a basis upon which models of chloride–DBDS interactions can be judged. We find that chloride increases the dissociation constant of DBDS from band 3 and also increases the rate at which DBDS binds to band 3. These data exclude a simple competitive interaction between chloride and DBDS. We have proposed a model in which chloride and DBDS have distinct, interacting binding sites. While this model is not unique, it satisfies the constraints imposed by the data.

We thank Mr. Benard Corrow for construction and maintenance of the equipment used in this project, Mr. Kevin Smith for technical help, and Ms. Donna Dilley for expert typing. Supported by NIH grants HL29488, HL14820 and GM00782.

References

Barzilay, M., Ship, S., Cabantchik, Z.I. 1979. Anion transport in red cells. II. Kinetics of reversible inhibition by nitroaromatic sulfonic acids. *Membr. Biochem.* **2**:255–281

Brown, A.S. 1934. A type of silver chloride electrode suitable for use in dilute solutions. *J. Am. Chem. Soc.* **56**:646–647

Cabantchik, Z.I., Knauf, P.A., Rothstein, A. 1978. The anion transport system of the red blood cell. The role of membrane protein evaluated by the use of "probes." *Biochim. Biophys. Acta* **515**:239–302

Cabantchik, Z.I., Rothstein, A. 1972. The nature of the membrane sites controlling anion permeability of human red blood cells as determined by studies with disulfonic stilbene derivatives. *J. Membrane Biol.* **10**:311–330

Dalmark, M. 1976. Effects of halides and bicarbonate on chloride transport in human red cells. *J. Gen. Physiol.* **31**:145–164

Dix, J.A., Verkman, A.S., Solomon, A.K., Cantley, L.C. 1979. Human erythrocyte anion exchange site characterised using a fluorescent probe. *Nature (London)* **282**:520–522

Dodge, J.T., Mitchell, C., Hanahan, D.J. 1963. The preparation and chemical characteristics of hemoglobin-free ghosts of human erythrocytes. *Arch. Biochem. Biophys.* **100**:119–130

Eigen, M., DeMayer, L. 1974. Theoretical basis of relaxation spectrometry. *In:* Investigation of Rates and Mechanisms of Reactions. G.G. Hammes, editor. Third edition, pp. 63–146. Wiley-Interscience, New York

Forman, S.A., Verkman, A.S., Dix, J.A., Solomon, A.K. 1982. Interaction of phloretin with the anion transport protein of the red blood cell membrane. *Biochim. Biophys. Acta* **689**:531–538

Fröhlich, O. 1982. The external anion binding site of the human erythrocyte anion transporter: DNDS binding and competition with chloride. *J. Membrane Biol.* **65**:111–123

Gunn, R.B., Fröhlich, O. 1979. Asymmetry in the mechanism for anion exchange in human red blood cell membranes. Evidence for reciprocating sites that react with one transported anion at a time. *J. Gen. Physiol.* **74**:351–374

Knauf, P.A. 1979. Erythrocyte anion exchange and the band 3 protein: Transport kinetics and molecular structure. *Curr. Top. Membr. Transp.* **12**:249–363

Knauf, P.A., Law, F.-L., Tarshis, T., Furuya, W. 1984. Effects of the transport conformation of the binding of external NAP-taurine to the human erythrocyte anion exchange system. *J. Gen. Physiol.* **83**:681–701

Knauf, P.A., Mann, N.A. 1984*a*. Location of the modifier site of the erythrocyte anion exchange system. *Biophys. J.* **45**:18a

Knauf, P.A., Mann, N.A. 1984*b*. Use of niflumic acid to determine the nature of the asymmetry of the human erythrocyte anion exchange system. *J. Gen. Physiol.* **83**:703–725

Kotaki, M., Naoi, R., Yagi, R. 1971. A diaminostilbene dye as a hydrophobic probe for proteins. *Biochim. Biophys. Acta* **229**:547–566

Lepke, S., Fasold, H., Pring, M., Passow, H. 1976. A study of the relationship between inhibition of anion exchange and binding to the red blood cell membrane of 4,4′-diisothiocyano stilbene-2,2′-disulfonic acid (DIDS) and its dihydro derivative (H_2DIDS). *J. Membrane Biol.* **29**:147–177

Lowry, O.H., Rosebrough, N.J., Farr, A.L., Randall, R.J. 1951. Protein measurement with the Folin phenol reagent. *J. Biol. Chem.* **193**:265–275

Macara, I.G., Cantley, L.C. 1981. Location of binding sites on the anion exchange protein of human erythrocytes: Evidence

for coexisting sites on opposite sides of the plasma membrane. *Biochemistry* **20**:5695–5701

Rao, A., Martin, P., Reithmeier, R.A.F., Cantley, L.C. 1979. Location of the disulfonic stilbene binding site of the human erythrocyte anion exchange system by fluorescence energy transfer. *Biochemistry* **18**:4505–4516

Robinson, R.A., Stokes, R.H. 1959. Electrolytic Solutions (2nd edition). Butterworths, London

Salhany, J.M., Gaines, E.D., Sullivan, R. 1981. Steady and transient state kinetics of erythrocyte anion exchange. Evidence for cooperativity in substrate and inhibitor binding suggesting site-site interactions within the band 3 protein dimer. *Biophys. J.* **33**:3a

Segel, I. 1975. Enzyme Kinetics, Behavior and Analysis of Rapid Equilibrium and Steady-State Enzyme Systems. John Wiley and Sons, New York

Shami, Y., Rothstein, A., Knauf, P.A. 1978. Identification of the Cl^- transport site of human red blood cells by a kinetic analysis of the inhibitory effects of a chemical probe. *Biochim. Biophys. Acta* **508**:357–363

Steck, T.L. 1978. The band 3 protein of the human red cell membrane: A review. *J. Supramol. Struct.* **8**:311–324

Verkman, A.S., Dix, J.A., Solomon, A.K. 1983. Anion transport inhibitor binding to band 3 in red blood cell membranes. *J. Gen. Physiol.* **81**:421–449

Received 31 January 1985; revised 27 August 1985

Appendix

Derivation of Equation (11)

We wish to derive a relation between τ, the stopped-flow time constant, and [DBDS] and [Cl]. The noncompetitive mechanism given in Eq. (6) will be used.

In stopped-flow experiments, DBDS is mixed with ghosts and the resultant exponential time course, $A = A_\infty(1 - e^{-t/\tau})$, is measured. In order to calculate τ as a function of [Cl], [DBDS] and the model parameters K_1, k_2, k_{-2}, K_1', k_2', k_{-2}' and K_{Cl}, we observe

$$1/\tau = (dA/dt)_{t=0}/(A)_{t=\infty} \tag{A.1}$$

where A is the sum of species present after the conformational change has occurred,

$$A = [b3^*DB] + [b3^*DBCl]. \tag{A.2}$$

It is clear from Eq. (6) that

$$(dA/dt)_{t=0} = k_2[b3DB] + k_2'[b3DBCl]. \tag{A.3}$$

Equation (3) can be simplified using the equilibrium relations given in Eq. (7) and the conservation condition, $[b3_{tot}] = [b3] + [b3Cl] + [b3DB] + [b3DBCl]$,

$$\left(\frac{dA}{dt}\right)_{t=0} = \frac{[b3_{tot}][DB]\left(\frac{k_2}{K_1} + \frac{k_2'[Cl]}{K_1'K_{Cl}}\right)}{1 + \frac{[DB]}{K_1} + \frac{[DB][Cl]}{K_1'K_{Cl}} + \frac{[Cl]}{K_{Cl}}}. \tag{A.4}$$

An expression for $(A)_{t=\infty}$ can be calculated from Eq. (A.2) and Eq. (7) using the conservation condition valid at equilibrium, $[b3_{tot}] = [b3] + [b3Cl] + [b3DB] + [b3DBCl] + [b3^*DBCl] + [b3^*DB]$,

$$(A)_{t=\infty} = \frac{[b3_{tot}][DB]\left(\frac{K_2}{K_1} + \frac{K_2'[Cl]}{K_1'K_{Cl}}\right)}{1 + \frac{[DB]}{K_{eq}} + \frac{[DB][Cl]}{K_{eq}'K_{Cl}} + \frac{[Cl]}{K_{Cl}}}. \tag{A.5}$$

Combining Eqs. (A.1), (A.4) and (A.5) gives Eq. (11) in the text.

Derivation of Hunter-Downs Relation

We wish to derive the appropriate Hunter-Downs relation for the mechanism given in Fig. 6 of the form

$$[DBDS](1 - i)/i = A[Cl] + B \tag{A.6}$$

where i is the fractional inhibition of transport, and A and B are functions of K_1, k_2, k_{-2}, K_1', k_2', k_{-2}', K_{Cl_o}, K_{Cl_i}, K_{oi}, $[Cl_o]$ and $[Cl_i]$.

Using the notation $[b3_iCl]_-$ as the $b3_iCl$ concentration in the presence of the inhibitor DBDS, and $[b3_iCl]_-$ as that in the absence of DBDS,

$$i = 1 - [b3_iCl]_+/[b3_iCl]_- \tag{A.7}$$

$$(1 - i)/i = [b3_iCl]_+/([b3_iCl]_- - [b3_iCl]_+). \tag{A.8}$$

The quantities $[b3_iCl]_-$ and $[b3_iCl]_+$ can be derived from the relations in Eq. (7) and the conservation conditions $[b3_{tot}] = [b3_o] + [b3_oCl] + [b3_i] + [b3_iCl]$ and $[b3_{tot}] = [b3_o] + [b3_oCl] + [b3_i] + [b3_iCl] + [b3DB] + [b3^*DB] + [b3DBCl] + [b3^*DBCl]$, respectively,

$$[b3_iCl]_- = \frac{[b3_{tot}]}{1 + K_{oi} + K_{oi}\frac{K_{Cl_o}}{[Cl_o]} + \frac{K_{Cl_i}}{[Cl_i]}} \tag{A.9}$$

$$[b3_iCl]_+ = \frac{[b3_{tot}]}{1 + K_{oi}\left(1 + \frac{[DB]}{K_{eq}'}\right) + K_{oi}\frac{K_{Cl_o}}{[Cl_o]}\left(1 + \frac{[DB]}{K_{eq}'}\right)}. \tag{A.10}$$

Combining Eqs. (A.8)–(A.10),

$$\frac{[DB](1 - i)}{i} = \frac{1 + K_{oi}\left(1 + \frac{K_{Cl_o}}{[Cl_o]} + \frac{K_{Cl_i}}{[Cl_i]}\right)}{K_{oi}\left(\frac{1}{K_{eq}'} + \frac{K_{Cl_o}}{[Cl_o]K_{eq}}\right)}. \tag{A.11}$$

When $[Cl_i] \gg [Cl_o]$, then Eq. (A.11) predicts that the $-x$ intercept of a Hunter-Downs plot will be

$$K_{(Cl_i - Cl_o)} = K_{oi}K_{Cl_o}/(1 + K_{oi}); \tag{A.12}$$

when $[Cl_i] = [Cl_o]$, then Eq. (A.11) predicts that the $-x$ intercept will be

$$K_{(Cl_i = Cl_o)} = (K_{oi}K_{Cl_o} + K_{Cl_i})/(1 + K_{oi}). \tag{A.13}$$

The ratio of the $-x$ intercept with chloride equal on both sides of the membrane to the $-x$ intercept with inside chloride much greater than outside chloride gives the asymmetry ratio, A

$$K_{(Cl_i = Cl_o)}/K_{(Cl_i \gg Cl_o)} = 1 + K_{Cl_i}/K_{oi}K_{Cl_o} = (1 + A)/A \tag{A.14}$$

where

$$A = K_{oi}K_{Cl_o}/K_{Cl_i}. \tag{A.15}$$

In the case of competitive interaction between DBDS and chloride, Fig. 6 becomes

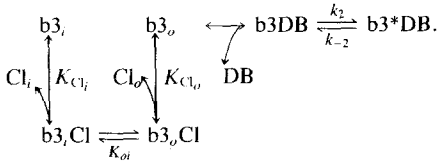

(A.16)

Equation (A.9) for $[b3_iCl]$ is unchanged since it is independent of inhibitor interaction, whereas the form for $[b3_iCl]_+$ becomes

$$[b3_iCl]_+ = \frac{[b3_{tot}]}{1 + K_{oi} + K_{oi}\dfrac{K_{Cl_o}}{[Cl_o]}\left(1 + \dfrac{[DB]}{K_{eq}}\right)\dfrac{K_{Cl_i}}{[Cl_i]}}. \tag{A.17}$$

The Hunter-Downs equation for the competitive mechanism in Eq. (A.16) becomes

$$[DB]_i(1 - i) = \frac{1 + K_{oi}\left(1 + \dfrac{K_{Cl_o}}{[Cl_o]}\right) + \dfrac{K_{Cl_i}}{[Cl_i]}}{\dfrac{K_{oi}K_{Cl_o}}{K_{eq}[Cl_o]}}. \tag{A.18}$$

Equation (A.18) gives identical $-x$ intercepts as the $-x$ intercepts of the mixed-inhibition mechanism in Fig. 6.

A similar derivation for K^{app} as a function of parameters in Fig. 6 gives an equation that is identical to the equation for the Hunter-Downs plot for the mixed-inhibition mechanism, Eq. (A.11). The reason is that the quantity $[I](1 - i)/i$ gives an apparent inhibitor dissociation constant in the presence of substrate.

For the case of $[Cl_o] = [Cl_i]$, Eq. (A.11) reduces to

$$K_{app} = \frac{\dfrac{K'_{eq}}{K_{oi}}([Cl] + K_{oi}([Cl] + K_{Cl_o}) + K_{Cl_i})}{[Cl] + \dfrac{K_{Cl_o}K'_{eq}}{K_{eq}}} \tag{A.19}$$

from which the chloride concentration at which K^{app} half-saturates, K^*_{Cl}, is $K_{oi}K'_{eq}/K_{eq}$, given in Eq. (10) of the text.

Analysis of Fluorescence Equilibrium Binding Data

The binding of DBDS to ghosts in the presence of chloride is described by a single-site mechanism; in the limit of excess DBDS, the concentration of bound forms of DBDS is related hyperbolically to the total DBDS concentration:

$$[bound] = [b3_{tot}][DBDS])/(K_{eq} + [DBDS]). \tag{A.20}$$

If all bound forms fluoresce with equal quantum yield, then the fluorescence, F, neglecting scattering, inner filter and self-quenching effects, is equal to the sum of contributions from bound fluorphore and free fluorphore by

$$F = \alpha[bound] + \beta[DBDS] \tag{A.21}$$

where α and β are proportionality constants containing the quantum yield of bound and free forms of DBDS as well as total site stoichiometry. We have been able to fit our equilibrium binding data very well assuming all forms of bound DBDS fluoresce with equal quantum yield. Furthermore, the quantum yield of bound DBDS appears not to depend on chloride, since the value of α is constant over a 0 to 600 mM range of chloride concentrations.

Scattering corrections add a constant, S, to the fluorescence. Inner filter and self-quenching effects reduce the fluorescence by an amount dependent on [DBDS]. In order to correct for these effects, we have measured the fluorescence of DBDS in the absence of ghosts and with the same instrumental settings as with ghosts, and have fit the resulting data to a quadratic function

$$F_{obs} = A[DBDS]^2 + \beta[DBDS] \tag{A.22}$$

where F_{obs} is the observed fluorescence and the coefficient A is negative, corresponding to saturation of the fluorescence. The quadatic function fit the data exceptionally well. The ratio of observed fluorescence to true fluorescence in these experiments is

$$F_{obs}/F = (\beta + [DBDS])/\beta = 1/Q. \tag{A.23}$$

Thus the observed fluorescence is reduced by a factor of $1/Q$ due to inner filter and self-quenching effects. Combining Eqs. (A.20) through (A.23), and including scattering effects, the observed fluorescence is

$$F_{obs} = Q^{-1}(\alpha[DBDS]/(K_{eq} + [DBDS]) + \beta[DBDS] + S) + C \tag{A.24}$$

where C is an instrumental offset. This equation differs from the equation published previously in the appendix to Verkman et al. (1983) which contained an error. The inner filter correction, Q, appears in Eq. (A.24) as $1/Q$. Values of Q ranged from 1.00 to 1.01 for [DBDS] < 400 nM, and were equal to 1.18 at 4 μM.

Equation (A.24) was fit by the nonlinear least-squares method to observed fluorescence values obtained by adding aliquots of DBDS to a ghost membrane solution. For the fit, Q and β were held fixed to values determined by parallel titrations performed in the absence of ghosts and fit by Eqs. (A.22) and (A.23); values of Q were calculated for each [DBDS] used in the ghost titration.